PHYSICAL REVIEW A **106**, 043108 (2022)

Thomas–Reiche–Kuhn correction for truncated configuration-interaction spaces: Case of laser-assisted dynamical interference

Mattias Bertolino,[1] Stefanos Carlström,[1] Jasper Peschel,[1] Felipe Zapata,[1]
Eva Lindroth,[2] and Jan Marcus Dahlström[1]
[1]*Department of Physics, Lund University, Box 118, SE-221 00 Lund, Sweden*
[2]*Department of Physics, Stockholm University, AlbaNova University Center, SE-106 91 Stockholm, Sweden*

(Received 14 July 2022; accepted 8 September 2022; published 14 October 2022)

The Thomas–Reiche–Kuhn sum rule is used to form an effective potential that is added to the time-dependent configuration-interaction singles (TDCIS) equations of motion in velocity gauge. The purpose of the effective potential is to include virtual coupling from singles to doubles, which is required for size-consistent velocity-gauge TDCIS results. The proposed method is compared to length-gauge TDCIS results for laser-assisted photoionization. Finally, a dynamical interference effect controlled by two-color fields is predicted for atomic targets.

DOI: 10.1103/PhysRevA.106.043108

I. INTRODUCTION

There are several frontiers of research in attosecond physics [1], including studies of charge migration in biorelevant molecules [2], generation of attosecond pulses in solid-state targets [3], and atomic delay measurements in laser-assisted photoionization [4]. It has been shown that attosecond precision measurements can be performed by photoelectron interferometry, using various forms of extreme ultraviolet (XUV) and infrared (IR) pulses, in atoms [4–8], molecules [9,10], and solids [11,12]. While this type of nonlinear interferometry can be qualitatively understood using the strong-field approximation, as we have recently reviewed in Ref. [13] for numerous experiments with light from high-order harmonic generation (HHG) and free-electron laser (FEL) sources, a more detailed interpretation requires the use of advanced many-body theory. In cases where the interaction with the fields is *weak* it is possible to employ perturbation theory to interpret attosecond delays from atoms [14,15], molecules [16–18], and laser-stimulated transitions via autoionizing states [19–24]. However, when the interaction with fields increase in strength, time-dependent simulations are essential to understand the correlation effects that accompany the laser-driven dynamics. Brute force approaches for photoionization studies are possible only in two-electron systems, such as He and H^-, where the Schrödinger equation can be directly propagated [25,26]. In other systems, time-dependent simulations of multielectron dynamics are more costly and one must rely on approximations that balance precision against the numerical cost. A few examples include the time-dependent configuration-interaction singles (TDCIS) [27,28], *R*-matrix [29,30], X-CHEM [24,31], and self-consistent field theories [32–34]. The latter theories rely on time-dependent Slater determinants, which form eigenstates of approximate time-dependent Hamiltonians. The simplest such example is the time-dependent Hartree–Fock (TDHF) theory, where a single Slater determinant is constructed from time-dependent occupied orbitals.

In addition to the level of electron correlation included in the simulations, care must also be given to the question of gauges that describe the electromagnetic interaction with the electrons. If no approximations were made, the Schrödinger equation could have equivalently been expressed in either gauge. However, the truncation of the basis makes the physical observables gauge-dependent [35–37]. This raises the question of which gauge happens to give (i) the best correspondence to experiment and (ii) the most convenient numerical properties. While the Hartree–Fock equations (HF) have been shown to be gauge invariant [38], such a formulation requires the occupied orbitals to be gauge-transformed dynamically in the presence of time-dependent fields. This implies that self-consistent field theories [32–34] are highly desirable in this regard, but unfortunately such theories are costly to propagate numerically. According to Kobe's gauge theory [39], the length gauge is unique with expansion coefficients that are genuine probability amplitudes. This implies that dynamic gauge transformations are less essential and that more efficient basis truncations can be performed in the length gauge, as compared to any other gauge. However, the length gauge is notorious for being difficult to converge for strong-field processes with low-frequency laser pulses [40–43]. Indeed, a relatively low number of angular momenta is required for convergence of TDCIS [27,28] in velocity gauge to describe laser-assisted photoionization [13,44]. On the other hand, length-gauge TDCIS calculations have empirically proven better than velocity-gauge calculations

[45], in agreement with the gauge theory of Kobe [38,39]. This means that when numerical convergence within the configuration-interaction singles (CIS) subspace is reached, the length-gauge results are more accurate than the velocity gauge results. To overcome this gauge problem in TDCIS, Sato *et al.* have developed a modification to TDCIS in velocity gauge by successively rotating the orbitals in each time step, effectively defining time-dependent orbitals, which are necessary for gauge invariance with the length-gauge TDCIS results [38,45].

In this article, we investigate the gauge-dependence problem in TDCIS, from a different perspective than Sato *et al.* [45], by bridging the space of single excitations to that of virtual double excitations. This is done by systematically adjusting for the lack of *core* polarization of excited states in TDCIS. In Sec. II, a review of polarization effects in N-electron atoms is presented by usage of the Thomas–Reiche–Kuhn (TRK) sum rule (see, e.g., Ref. [46]). We then introduce an effective potential of the TRK-type to the equations of motion for velocity-gauge TDCIS in Sec. III. In Sec. IV, results for laser-assisted photoionization are presented for velocity-gauge TDCIS and the proposed TDCIS-TRK theory. It is shown that TDCIS-TRK provides accurate results where velocity-gauge TDCIS fails. We also revisit dynamical interference in photoionization [47–49] and predict that the phenomenon is experimentally feasible in a new setting with two-color fields. Finally, in Sec. V we conclude our findings.

II. THEORY

An atom subject to an external laser field will have its dynamics ruled by the minimal coupling Hamiltonian

$$\hat{H}(\mathbf{r},t) = \hat{H}_0 + \hat{V}_1(\mathbf{r},t) + \hat{V}_2(\mathbf{r},t), \tag{1}$$

where the zeroth term $\hat{H}_0$ is the atomic Hamiltonian, which accounts for the kinetic energy and the Coulomb interaction with the nucleus and among the electrons. For a wavelength substantially larger than the atom, $\lambda \gg a_0$, the spatial dependence of the field can be neglected. This is referred to as the dipole approximation, and when applied to the minimal coupling Hamiltonian, we refer to it as the *velocity gauge*. The interactions with the electromagnetic field are hence given by a term linear in the time-dependent vector potential,

$$\hat{V}_1(t) = -\frac{q}{m}\mathbf{A}(t)\cdot\sum_{ij}\mathbf{p}_{ij}\hat{c}_i^\dagger\hat{c}_j, \tag{2}$$

and a term quadratic in the vector potential,

$$\hat{V}_2(t) = \frac{q^2A^2(t)}{2m}\hat{n}. \tag{3}$$

Here, $q=-e$ is the electronic charge and $\mathbf{p}_{ij} = \langle i|\hat{\mathbf{p}}|j\rangle$ denotes the matrix element for momentum between the canonical orbitals i and j, which are eigenstates of the mean-field (Fock) operator $\hat{f}|i\rangle = \varepsilon_i|i\rangle$. The operators $\hat{c}_i^\dagger$ and $\hat{c}_i$, create and annihilate an electron in the canonical orbital i, respectively. The $\hat{V}_2$ operator acts as a scalar, due to any N-body state being an eigenstate to the number operator $\hat{n} = \sum_i \hat{c}_i^\dagger\hat{c}_i$, such that $\hat{n}|\Psi\rangle = N|\Psi\rangle$.

A. Energy shifts in an oscillating potential

Consider a monochromatic vector potential $A(t) = A_0\cos(\omega t)$, polarized linearly along the z axis. The potential term linear in the vector potential is given by

$$\hat{V}_1(t) = \hat{V}_1^{(+)}\exp(-i\omega t) + \hat{V}_1^{(-)}\exp(i\omega t), \tag{4}$$

with

$$\hat{V}_1^{(+)} = \hat{V}_1^{(-)} = -\frac{q}{2m}A_0\sum_{ij}(p_z)_{ij}\hat{c}_i^\dagger\hat{c}_j, \tag{5}$$

where the superscripts $(+)$ and $(-)$ correspond to interactions that induce absorption and emission of a photon, respectively. The quadratic potential amplitude is given by

$$\hat{V}_2(t) = \frac{q^2A_0^2\cos^2(\omega t)}{2m}\hat{n}. \tag{6}$$

The second-order energy correction to any N-electron state, $|\Psi_0\rangle$, due to $\hat{V}_1(t)$ is given by

$$\left\langle \Delta E_1^{(2)}(\omega)\right\rangle = \lim_{\eta\to 0^+}\sum\!\!\!\!\!\!\int_{n\neq 0}\left(\frac{\langle\Psi_0|\hat{V}_1^{(+)}|\Psi_n\rangle\langle\Psi_n|\hat{V}_1^{(-)}|\Psi_0\rangle}{E_0-\hbar\omega-E_n+i\eta} + \frac{\langle\Psi_0|\hat{V}_1^{(-)}|\Psi_n\rangle\langle\Psi_n|\hat{V}_1^{(+)}|\Psi_0\rangle}{E_0+\hbar\omega-E_n+i\eta}\right), \tag{7}$$

which can be interpreted as a level shift of the state averaged over time [50]. The TRK sum rule states that the sum of all oscillator strengths, $f_{nn'}$, from a particular atomic eigenstate, $|\Psi_n\rangle$, is equal to the number of electrons:

$$\sum_{n'} f_{nn'} = \sum_{n'}\frac{2m}{\hbar^2}(E_n - E_{n'})|\langle\Psi_{n'}|\hat{z}|\Psi_n\rangle|^2 = N. \tag{8}$$

The application of TRK theory to Eq. (7) requires that the commutation between the atomic Hamiltonian and the dipole operator equals the momentum operator, $[\hat{H}_0,\hat{z}] = -i\hbar\hat{p}_z/m$, (see, e.g., Eq. (61.1) in Ref. [51]). Since this condition is satisfied for any *local* potential, the TRK sum rule can be used to perform exact calculations in N-electron atoms, where all interactions are inherently local. The time-averaged energy shift to second order in $\hat{V}_1(t)$ is derived from the TRK sum rule in Eq. (8) with a Taylor expansion of the denominators in Eq. (7) with $\hbar\omega \ll |E_n - E_0|$ to yield

$$\left\langle \Delta E_1^{(2)}(\omega)\right\rangle = -\frac{A_0^2}{4}\left(\frac{q^2}{m}N + \omega^2\alpha_0\right) + O(\omega^4), \tag{9}$$

where

$$\alpha_0 = \frac{q^2\hbar^2}{m}\sum_{n\neq 0}\frac{f_{n0}}{(E_0-E_n)^2} \tag{10}$$

is the atomic *polarizability*, as defined in Ref. [52]. The time-averaged energy shift of the first-order energy correction due to the quadratic term $\hat{V}_2(t)$ is simply given by

$$\left\langle \Delta E_2^{(1)}(\omega)\right\rangle = \frac{q^2\langle A^2(t)\rangle}{2m}N = \frac{q^2A_0^2}{4m}N. \tag{11}$$

This shows that, in the case of a monochromatic field, the energy corrections due to $\hat{V}_1(t) + \hat{V}_2(t)$ to second order in the vector potential *cancel* such that the explicit N dependence in the energy shift disappears. The remaining energy shift in the velocity gauge is

$$\langle \Delta E^{(2)}(\omega)\rangle = -\frac{\omega^2 A_0^2 \alpha_0}{4} + O(\omega^4) = -\frac{E_0^2\alpha_0}{4} + O(\omega^4), \tag{12}$$

which can be found more easily in the length gauge with the electric field $E(t) = -\frac{dA}{dt} = E_0 \sin(\omega t)$ by second-order perturbation theory with the dipole operator $\hat{V}_1^{(\text{len.})} = -qE(t)\hat{z}$. While the length gauge is simpler in this regard, because it does not rely on a detailed cancellation effect of two different perturbation terms, the energy shifts are found to be equivalent in both gauges. We stress that this exact result is general, as it applies to any state in atomic or molecular targets, but it fails in cases where the considered state resonates with another state at the applied frequency: $\hbar\omega \approx |E_n - E_0|$. Thus, as pointed out by Bucksbaum *et al.* [53], it is typically an excellent approximation for the ground state of an atom, or molecule, subject to a low-frequency laser field, $\hbar\omega \ll |E_n - E_0|$, but it is a bad approximation for excited states, where other Rydberg states are likely to be close in energy. We note that the TRK rule has been used in solids to reduce the necessary number of energy bands in the velocity gauge while ensuring convergence [54]. In the present work, however, we make use of the TRK sum rule in the numerical propagation to correct for size inconsistency in virtual excitations that are missing due to truncations of the many-body configuration-interaction expansion.

B. Configuration interaction (CI)

Many-body effects can be described by time-dependent configuration-interaction (TDCI) methods, where the total electron wave function is expanded as

$$|\Psi(t)\rangle = \alpha_0(t)|\Phi_0\rangle + \sum_{ap} \alpha_a^p(t)\big|\Phi_a^p\big\rangle + \sum_{abpq} \alpha_{ab}^{pq}(t)\big|\Phi_{ab}^{pq}\big\rangle + \cdots, \tag{13}$$

where $|\Phi_0\rangle$ denotes the HF reference Slater determinant, while $|\Phi_a^p\rangle$ and $|\Phi_{ab}^{pq}\rangle$ denote single and double excitations, respectively. The labels $a, b, \ldots$ index the occupied orbitals, and the labels $p, q, \ldots$ index the unoccupied orbitals in the initial reference state. While the orbitals are found variationally, without the laser-action part of the Hamiltonian, the expansion coefficients $\alpha(t)$ are time-dependent quantities in TDCI methods. The expansion in Eq. (13) can be truncated in several ways. If the expansion is truncated so that the CI space is limited to the level of single excitations it is known as TDCIS [27,28]. The singly excited states $|\Phi_a^p\rangle$ are in the nonrelativistic case restricted to the spin-singlet state character constructed using second quantization as

$$|\Phi_a^p\rangle = \frac{1}{\sqrt{2}}\{\hat{c}_{p+}^\dagger \hat{c}_{a+} + \hat{c}_{p-}^\dagger \hat{c}_{a-}\}|\Phi_0\rangle. \tag{14}$$

The operator $\hat{c}_{p\sigma}^\dagger$ creates an electron in the virtual orbital p with spin σ and the operator $\hat{c}_{a\sigma}$ creates a hole in the core orbital a with spin σ. While TDCI methods imply that occupied orbitals are static eigenstates of a laser-free mean-field Hamiltonian, electronic excitations at the TDCIS level can be interpreted as time-dependent wave packets in the form of superpositions of initially unoccupied orbitals [27]. Recently, implementations of TDCIS that are not restricted to spin-singlet configurations have been realized, e.g., one in the form of two-component orbitals from relativistic pseudopotentials [55,56], and another based on the four-component orbitals from the Dirac-Fock equation [57]. In the following work we consider only the spin-singlet configurations and linearly polarized fields, such that the magnetic quantum number is conserved: $m_p = m_a$, where in addition the *gerade* symmetry of TDCIS can be utilized to further reduce the number of correlated channels [58]. Further truncation in CI can be performed to limit the allowed excitations, e.g., *freezing* occupied orbitals corresponding to tightly bound electrons (cf. Refs. [32–34,59,60]).

C. Application of TRK sum rule to TDCIS

Truncation of the Hilbert space implies that the TRK sum rules will not hold. Nonetheless, we consider the CI space to be truncated at the level of single excitations (CIS), where the states in Eq. (7) are given by the space spanned by the HF ground state and the CIS singly excited states, $\{|\Psi_0\rangle, |\Psi_n\rangle\} \rightarrow \{|\Phi_0\rangle, |\Phi_a^p\rangle\}$, respectively. We denote the space of no excitations by $\mathcal{P}_0$, single excitations by $\mathcal{P}_1$, and double excitations by $\mathcal{P}_2$. In Fig. 1, we illustrate some processes from perturbation theory, represented as Goldstone diagrams, that give rise to energy shifts due to the second-order action of $\hat{V}_1(t)$. Figure 1(a) can be interpreted as an uncorrelated (bare) energy correction of the HF ground state, $|\Phi_0\rangle$ in $\mathcal{P}_0$, due to a virtual transition via the singly excited state $|\Phi_a^p\rangle$ in $\mathcal{P}_1$. Since in TDCIS theory both $\mathcal{P}_0$ and $\mathcal{P}_1$ are contained in the truncated Hilbert space, the polarization of the HF ground state will be reasonably well described. The singly excited states can also shift their energies due to second-order action with $\hat{V}_1(t)$ within $\mathcal{P}_1$ and via $\mathcal{P}_0$. These effects are described in TDCIS theory, as shown in Figs. 1(b)–1(d). However, some perturbative processes that also change the energy of the singly excited states are missing, since they require a virtual transition via the *doubly* excited states in $\mathcal{P}_2$, as shown in Figs. 1(e)–1(g). Figure 1(e) shows that the laser field can polarize the core of the atom, similar to how the ground state was excited [Fig. 1(a)], which leads to an energy shift of ∼N, in accordance with Eq. (9). However, the atomic core is missing one-electron *exchange* processes [Figs. 1(f) and 1(g)] that impose the Pauli exclusion principle, which will reduce the core energy shift to ∼$N - 1$. Additionally, the reversed time order of Fig. 1(d) is also missing in CIS and further many-body polarization effects, induced by Coulomb interactions, must be carefully considered by many-body perturbation theory (MBPT) for accurate energy shifts.

Since the diagrams in Figs. 1(e)–1(g) are nonexistent in TDCIS, the time evolution will be subject to spurious effects. While the polarization effects are reasonably accounted for in the ground state, the excited states in CIS have an unbalanced polarization that lacks size consistency. Since transitions between the ground state and the excited states are essential in TDCIS theory, this inconsistency will result in largely

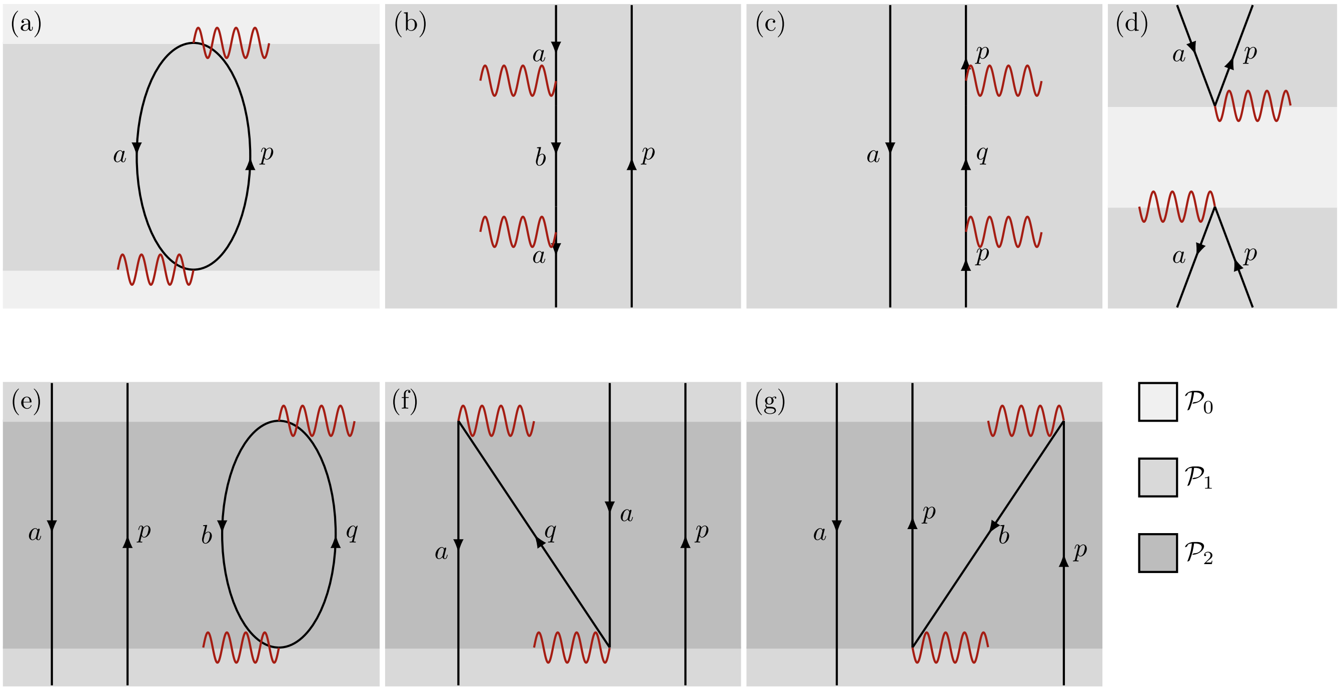

FIG. 1. Goldstone diagrams of the energy contributions within CIS [panels (a)–(d)] and CID [panels (e)–(g)]. The diagram in panel (a) describes the energy shift of the core, while the diagrams in panels (b)–(g) describe the energy shift of an excited CIS state. The background shading color indicates the CI space where the atom resides. Time flows upwards in these Goldstone diagrams.

overestimated relative energy shifts for excitations, with an unphysical dependence on the number of active electrons. These types of relative energy shifts are usually avoided in MBPT, by the linked diagram theorem (see, e.g., Ref. [61]), but in time-dependent simulations such as TDCIS the problem must be treated in a different way. We introduce an effective potential that corrects the relative energy shifts based on TRK theory. In order to understand this better we first consider the energy shifts computed for the HF ground state of neon with various approximations using MBPT.

Due to the nonlocality of the Hartree–Fock exchange potential, the second-order energy correction is not exactly given by Eq. (9) when static or frozen occupied orbitals are used. Instead, we define the ground-state energy shift

$$\left\langle \Delta\tilde{E}_1^{(2)}(\omega)\right\rangle = -\frac{A_0^2}{4}\left(\frac{q^2}{m}\tilde{N} + \omega^2\tilde{\alpha}_0\right) + O(\omega^4), \tag{15}$$

where $\tilde{N}$ and $\tilde{\alpha}_0$ denote the corresponding values of N and α_0 for a given approximation: lowest-order perturbation (LOP), CIS, and random-phase approximation with exchange (RPAE). The *effective* number of active electrons, which is a frequency-independent quantity, is computed as

$$\tilde{N} \equiv -\left(\frac{8m}{A_0^2 q^2}\right)\sum_a^{\text{occ.}}\langle a|\hat{V}_1|\rho_{0,a}^{(+)}\rangle, \tag{16}$$

where a label all occupied orbitals in the HF ground state and $|\rho_{0,a}^{(+)}\rangle$ is the associated perturbed wave function after one interaction with the field that depends on the level of approximation. In the case of RPAE, the perturbed wave functions are (in atomic units) constructed as (see Ref. [62])

$$\begin{aligned}|\rho_{\omega,a}^{(\pm)}\rangle = \sum_p^{\text{exc.}}\frac{|p\rangle}{\varepsilon_a-\varepsilon_p\pm\omega}\Bigg[\langle p|\hat{V}_1|a\rangle - \sum_b^{\text{occ.}}\Big(&\langle b,p|r_{12}^{-1}|a,\rho_{\omega,b}^{(\pm)}\rangle \\ &- 2\langle b,p|r_{12}^{-1}|\rho_{\omega,b}^{(\pm)},a\rangle + \langle\rho_{\omega,b}^{(\mp)},p|r_{12}^{-1}|a,b\rangle \\ &- 2\langle\rho_{\omega,b}^{(\mp)},p|r_{12}^{-1}|b,a\rangle\Big)\Bigg],\end{aligned} \tag{17}$$

where the superscripts $(+)$ and $(-)$ denote forward- and backward-propagating perturbed wave functions. Note that it is the $(+)$ function at zero frequency, $\omega = 0$, that is inserted into Eq. (16). The first $(+)$ term on the right-hand side of Eq. (17) corresponds to uncorrelated (bare) excitation, which we label as LOP. Including also the second and third $(+)$ terms corresponds to forward-propagating electron-hole correlations, which we label CIS, because it is the level of correlation obtained by solving TDCIS (also known as Tamm–Dancoff; see, e.g., Ref. [62]). The fourth and fifth terms are exclusive to RPAE and they correspond to ground-state correlation effects (direct and exchange) by self-consistent solution of both $(+)$ and $(-)$ terms. More details about the use of perturbed wave functions in attosecond physics, and how they correspond to dressing of the lower vertex in Fig. 1(a), are found in Refs. [14,15]. In Table I the numerically obtained values of $\tilde{N}$ for LOP, CIS, and RPAE are presented together with the number of active electrons in the core of neon atoms. RPAE is exceptional since it corresponds to the linear response of the TDHF approximation, which is a self-consistent field theory and therefore does obtain the correct number of electrons. However, when the active core is truncated to $N_{\text{A}} < N$, RPAE does *not* provide the correct number of active electrons. It is

TABLE I. Effective number of active electrons $\tilde{N}$ within LOP, CIS, and RPAE, for the neon atom ($1s^2 2s^2 2p^6$) given the number of electrons in the active core: N_A.

Active	$\tilde{N}_\text{LOP}$	$\tilde{N}_\text{CIS}$	$\tilde{N}_\text{RPAE}$	N_A
$2p$	5.4091	6.1758	7.2461	6
$2s, 2p$	6.2712	7.2558	8.3022	8
$1s, 2s, 2p$	7.8528	8.8858	10.0000	10

interesting to note that, when only $2p$ orbitals are active, the CIS approximation outperforms the RPAE approximation in this aspect.

D. Energy shifts in a static potential

Alternatively, static energy shifts of the HF ground state, $|\Phi_0\rangle$, in response to an external potential, $\hat{V}_1$, can be obtained by diagonalizing the Hamiltonian $\hat{H}_0 + \hat{V}_1$ expressed within CIS. In this case a constant static vector potential, $A^{(\text{stat.})} = A_0$, in the linear interaction term in Eq. (2) is used. Since the action of the quadratic term is trivial in this case it is omitted in the following discussion. This approach has the advantage that it is not restricted to the second-order interaction, but includes all higher-order corrections with the field directly. Diagonalization of the CIS Hamiltonian can also be used to study nonlinear DC Stark shifts of excited (Rydberg) states. This feature is, however, of limited use since laser fields with finite frequencies will induce AC Stark shifts that differ significantly from the DC results due to resonances in the Rydberg series.

In Fig. 2, we plot *half*-static energy shifts, $E_1^{(\text{stat.})}/2$, as a function the ponderomotive energy of an electron, $U_p = \frac{q^2 A_0^2}{4m}$, in an oscillating vector potential with the corresponding amplitude $A^{(\text{osci.})}(t) = A_0 \cos(\omega t)$. The half-static energy shifts of the HF ground state follow the time-averaged energy shifts, predicted by Eq. (9) with N substituted by $\tilde{N}_\text{CIS}$ from Table. I, as shown by solid lines, $-\tilde{N}_\text{CIS} U_p$. There is a factor of 2 difference between the static energy shifts and those predicted by Eq. (7) for monochromatic pulses because energy conservation is respected only by acting once with $\hat{V}_1^{(-)}$ and once with $\hat{V}_1^{(+)}$, in any time order, but not with twice the action of the same $\hat{V}_1^{(\pm)}$. In the limit $\omega \to 0$, however, conservation of energy is fulfilled for all four cases, yielding a factor of 2 compared to the time-averaged energy shift,

$$\Delta E_1^{(\text{stat.})} \approx 2\big\langle \Delta\tilde{E}_1^{(2)}(\omega \to 0)\big\rangle. \tag{18}$$

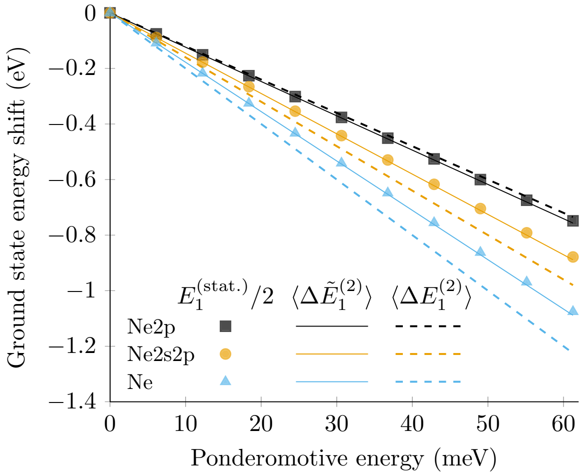

FIG. 2. Calculated polarization of the HF ground state of neon with an applied static vector potential in the velocity gauge with truncated space and full CIS space. Perturbation theory results are included as guiding lines.

At high ponderomotive energies, higher-order interactions with the static field lead to a slight disagreement with the perturbative results, $-\tilde{N}_\text{CIS} U_p$, as can be observed in Fig. 2. Energy shifts equal to $-N_\text{A} U_p$ are shown as dashed lines for reference. The significant discrepancy between the diagonalized ground-state energy shift in CIS and the exact TRK theory, $-N_\text{A} U_p$, originates from the truncations performed in the CI expansion, which leads to a nonlocal potential in TDCIS theory.

III. METHOD

A. Effective potential

Effective potentials have found several important applications in atomic, molecular, and optical physics. The key point is to reduce the complexity of a problem by replacing some degrees of freedom with a potential that depends on energy. Effective potentials can be employed to perform *self-energy correction* to holes, due to virtual Auger or shake-up processes or, more generally, to include virtual many-body interactions into a subspace $\mathcal{P}$ from a complement space $\mathcal{Q}$ [61,62]. Similarly, *optical potentials* are used in scattering theory to include virtual processes in the target that are induced by the impinging particle [63]. Effective potentials can also be used to include laser dressing effects, such as AC Stark shifts into a two-level system ($\mathcal{P}$), due to virtual interactions with the complement of the truncated Hilbert space ($\mathcal{Q}$) [64,65]. In this work, we introduce an effective potential that corrects for the lack of core polarization effects in the velocity-gauge formulation of TDCIS theory. We do this by adapting the TRK theory, discussed in Sec. II, to a time-dependent form where nonresonant virtual couplings to double excitations are incorporated to second order in the field. We make the following postulates for the core of $N-1$ electrons that remain after a single excitation from the ground state.

(i) *Markovian process.* The excitations from singles to doubles are virtual processes that only depend on the instantaneous value of the vector potential: $A(t)$, with no lasting memory effects in the state of the core over time.

(ii) *Nonresonant dynamics.* The energy shift of the core is described by nonresonant dynamics that can be evaluated by TRK theory as $-(N-1)q^2A^2(t)/2m$, at each given time t by virtual coupling from $\mathcal{P} = \mathcal{P}_1$ to $\mathcal{Q} = \mathcal{P}_2$.

(iii) *Nonlocal correspondence.* The effects of exchange interactions in TDCIS are adopted into the core energy shift using the following substitution: $N-1 \to \tilde{N}-1$, where $\tilde{N}$ is the effective number of active electrons in the HF ground state.

(iv) *Uniform action.* The core polarization energy affects all singly excited states in the same way independent of their individual energy and symmetry.

Using this set of assumptions, we postulate an effective potential for singles (S):

$$\hat{V}^{(\mathrm{S})}_{\mathrm{TRK}}(t) = \mathcal{V}_{\mathrm{TRK}}(t)\hat{P}_1 = -\frac{q^2}{2m}(\tilde{N}-1)A^2(t)\hat{P}_1, \tag{19}$$

where

$$\hat{P}_1 = \sum_{p}^{\text{virt.}}\sum_{a}^{\text{occ.}} \left|\Phi^p_a\right\rangle\left\langle\Phi^p_a\right| \tag{20}$$

is a $\mathcal{P}_1$ projector that acts on the singly excited states. The effective potential in Eq. (19) could be further improved by adding the polarization energy of the core, $-\alpha_0^{(N-1)}E^2(t)/2$, from Eq. (12) for the $N-1$ subsystem. We have *not* done this because that type of correction requires knowledge of the core system at a level that is *beyond* the CIS framework. We stress that such core polarization effects are also missing in the length-gauge formulation of TDCIS [see Fig. 1(e)]. We mention that it is straightforward to widen the present concept for generation of effective potentials that correct for virtual triples from doubles (D), $\hat{V}^{(\mathrm{D})}_{\mathrm{TRK}}(t)$, etc., but since such potentials are beyond TDCIS they are not considered in the present work.

B. Equations of motion

We define the CIS-TRK Hamiltonian as

$$\hat{H}_{\mathrm{TRK}} \equiv \hat{H}_{\mathrm{CIS}} + \hat{V}^{(\mathrm{S})}_{\mathrm{TRK}}, \tag{21}$$

where $\hat{H}_{\mathrm{CIS}}$ is the original CIS Hamiltonian for the velocity gauge [28,66]. Due to the closure of the CIS space, $\hat{I}_{\mathrm{CIS}} = \hat{P}_0 + \hat{P}_1$, the effective potential can be moved to instead act exclusively on the ground state. This is done by subtracting a time-dependent term from the CIS-TRK Hamiltonian:

$$\hat{H}'_{\mathrm{TRK}} \equiv \hat{H}_{\mathrm{TRK}} - \mathcal{V}_{\mathrm{TRK}}(t)\hat{I}_{\mathrm{CIS}} = \hat{H}_{\mathrm{CIS}} - \mathcal{V}_{\mathrm{TRK}}(t)\hat{P}_0,$$

where $\hat{P}_0 = |\Phi_0\rangle\langle\Phi_0|$. This substitution, $\hat{H}_{\mathrm{TRK}} \rightarrow \hat{H}'_{\mathrm{TRK}}$, can formally be interpreted as a time-dependent gauge transformation that will modify the phase of the wave functions, but not alter any physical observables generated from the CIS-TRK theory.

The TDCIS-TRK′ equations of motions are (in atomic units) written as

$$\begin{aligned} i\dot{\alpha}_0(t) &= \sqrt{2}A(t)\sum_{ap}\langle a|\hat{p}_z|p\rangle\alpha^p_a(t) + \frac{\tilde{N}-1}{2}A^2(t)\alpha_0(t),\\ i\dot{\alpha}^p_a(t) &= (\varepsilon_p - \varepsilon_a)\alpha^p_a(t) + \sum_{bq}\left[2\langle bp|r_{12}^{-1}|qa\rangle - \langle bp|r_{12}^{-1}|aq\rangle\right]\alpha^q_b(t)\\ &\quad + A(t)\left(\sqrt{2}\langle p|\hat{p}_z|a\rangle\alpha_0(t) + \sum_q\langle p|\hat{p}_z|q\rangle\alpha^q_a(t) - \sum_b\langle b|\hat{p}_z|a\rangle\alpha^p_b(t)\right), \end{aligned} \tag{22}$$

which differ only by the addition of the effective potential in the ground-state amplitude equation, when compared with the original TDCIS formulations [28,66]. In writing Eq. (22) we have omitted the $\hat{V}_2(t)$ operator, because it will affect *all* CIS states in the same way within the dipole approximation. As a result, it is possible to remove it without affecting any physical observable generated from the theory. We stress that the cost of implementing the TDCIS-TRK′ theory in Eq. (22) is only one *scalar* multiplication per time step in the numerical propagation. In Sec. IV, we show that this seemingly minor correction to the equations of motion have important implications for the TDCIS theory.

IV. RESULTS

In order to validate the action of the effective potential in Eq. (19), we perform *truncated* TDCIS simulations for laser-assisted photoionization for neon atoms with realistic pulse parameters corresponding to an XUV pulse and an IR laser pulse, as defined in Eq. (A1). The pulse duration is set to $\tau = 35$ fs, which is a typical value for XUV pulses generated by HHG or FEL. The properties of the IR field are chosen to correspond to a Ti:sapphire laser system. In general, the photoelectron peak position depends on the detailed pulse forms of both the IR and XUV fields in laser-assisted photoionization. This is because the ponderomotive energy,

$$U_p(t) \equiv U_p^0 f^2(t) \approx q^2\mathcal{A}^2_{\omega,0}(t)/4m, \tag{23}$$

with $\mathcal{A}_{\omega,0}(t) = A_{\omega,0}f(t)$, is dominated by the IR field, while the probability of one-photon ionization by the central XUV photon, Ω, depends on time through the squared envelope of the XUV field:

$$\dot{P} \sim |\mathcal{A}_{\Omega,0}(t)|^2 = |A_{\Omega,0}f(t)|^2. \tag{24}$$

In this way, the two fields have clearly defined roles: the IR field controls the dressing of the continuum, while the XUV field controls the flux of ejected electrons.

A. Energy shift of the photoelectron

In this subsection we consider the case where both the XUV and IR pulses have flat-top envelopes as defined in Eq. (A2). In Fig. 3(a), we show photoelectron probability distributions for absorption of one XUV photon from the neon

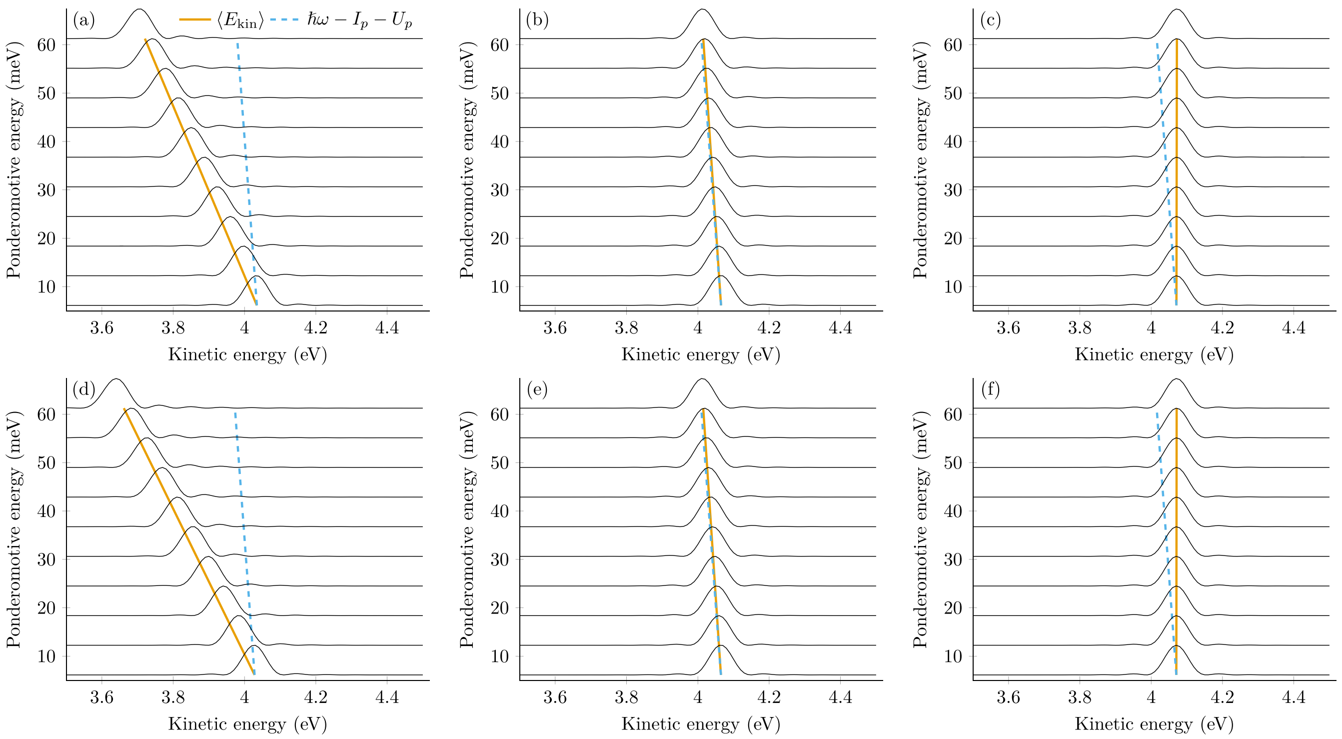

FIG. 3. Normalized photoionization spectra using velocity-gauge TDCIS in neon with the $2p$ orbitals active [panels (a)–(c)] and with the $2s$ and $2p$ orbitals active [panels (d)–(f)]. The solid lines show the measured peak position and the dashed lines show the expected peak position given by $\Delta E_{\mathrm{kin}} = -U_p$. The middle column [panels (b) and (e)] displays the velocity-gauge TDCIS-TRK with the effective potential $\hat{V}^{(\mathrm{S})}_{\mathrm{TRK}}$ and the rightmost column [panels (c) and (f)] displays the velocity-gauge TDCIS-TRK with the substitution $\tilde{N} - 1 \rightarrow \tilde{N}$.

ground state. Truncated TDCIS theory is used with only the $2p$ orbitals active. The intensity of the IR field is kept in the range $I = 10^{11}$ W/cm^2 to $I = 10^{12}$ W/cm^2, such that its main consequence is to assist the XUV photoionization process with the formation of sidebands (not shown), but also to shift the photoelectron structure to lower kinetic energies due to an increased ponderomotive potential [53]. A classical estimate for the kinetic energy of the photoelectron is given by $\langle E_{\mathrm{kin}} \rangle \approx \hbar\Omega + \varepsilon_{2p} - U_p^0$ (dashed sky blue line), where $\varepsilon_{2p} < 0$ is the energy of the $2p$ orbitals. As will be shown, this estimate is valid provided that both IR and XUV fields are flat-top pulses of the same duration, but with truncated TDCIS we instead observe a shift of the peak position of roughly $E_{\mathrm{kin}} \approx \hbar\omega + \varepsilon_{2p} - N_{\mathrm{A}} U_p^0$ (solid orange line), where $N_{\mathrm{A}} \approx 6$ because only the $2p$ orbitals are open. Obviously, this TDCIS shift is much too large when compared to the classical estimate. In order to understand the convergence properties of TDCIS, we expand the active space to include both $2s$ and $2p$ orbitals. This leads to an even stronger effect, as shown in Fig. 3(d), and thus worse agreement with the classical estimate. Finally, in the case where all orbitals are active, we find that the agreement with the classical prediction is further worsened (not shown). This proves that extending the active core of TDCIS to *full* TDCIS does not resolve the issue, but rather confirms that the major issue with the velocity-gauge TDCIS is a synthetic AC Stark shift due to size inconsistency.

In Figs. 3(b) and 3(e), we show the results of TDCIS-TRK theory, with the equation of motion defined in Eq. (22), for the truncated active cores: $\{2p\}$ and $\{2s, 2p\}$, respectively. It is observed that the photoelectron peak for single XUV absorption follows the expected classical prediction closely (dashed line). Furthermore, the two sets of simulations yield graphically equivalent results, which implies that the addition of the active $2s$ orbital was not essential to describe the physical process.

In order to study the role of the effective potential further, we make the substitution $\tilde{N} - 1 \rightarrow \tilde{N}$ in Eq. (22) and present the corresponding photoelectron peaks in Figs. 3(c) and 3(f), with active cores $\{2p\}$ and $\{2s, 2p\}$, respectively. Quite remarkably, it is found that the photoelectron peak now remains fixed at the same kinetic energy independent of the laser intensity. This (unphysical) substitution corresponds to neglecting that one electron is removed from the atom in the process of photoionization and it shows that the exact value of the effective number of active electrons, $\tilde{N}$ in Table I, is crucial to understand the ponderomotive shift of photoelectrons. In this way we have verified that the assumption of *nonlocal correspondence* between the $(N-1)$-body ionic core and the N-body atom is correct.

B. Comparison with length gauge

In this subsection we consider the case where the pulses have more realistic time-dependent envelopes, specifically given by the truncated Gaussian envelopes defined in Eq. (A3). Photoelectron probability distributions for one-photon ionization by an XUV field with an assisting laser field are shown using TDCIS-TRK theory in Fig. 4. A classical

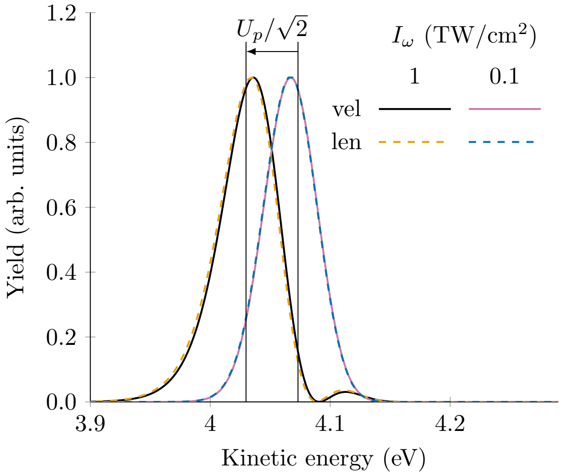

FIG. 4. One-photon peak of laser-assisted photoionization with a truncated Gaussian envelope using both TDCIS-TRK velocity gauge and length gauge. The expected classical energy shift for a Gaussian envelope is shown with an arrow labeled $U_p/\sqrt{2}$.

estimate of the mean kinetic energy shift of the photoelectron gives $\langle \Delta E_{\text{kin}} \rangle \approx -\Delta U_p^0/\sqrt{2}$, provided that both IR and XUV fields are Gaussian pulses of the same duration. The classical estimate for the photoelectron shift is marked with an arrow and shows good agreement with the numerical simulations. As expected from the classical estimates, the photoelectron peak shifts less when Gaussian pulses, instead of flat-top pulses, are employed. The quantum mechanical result shows a slightly smaller shift than the classical Gaussian estimate. Finally, we have verified that the photoelectron spectra from length-gauge TDCIS simulations (dashed lines) are in excellent agreement with the corresponding TRK results for the normalized yield. On the blue side of the high-intensity peak ($I_\omega = 10^{12}$ W/cm^2), we observe an interference ripple in both gauges. We propose that this phenomenon is the onset of dynamical interference due to ionization at the rising and the falling sides of the field, which is discussed in more detail in the following section.

C. Laser-assisted dynamical interference

In Ref. [48] two criteria to observe dynamical interference are put forward: (i) the relative AC Stark shift between the initial and final states needs to be larger than the bandwidth of the pulse, and (ii) the ionization rate should not be so large that the initial state is depleted on the rising side of the field. In practice, this makes the experimental observation of dynamical interference very challenging, as it must rely on atomic stabilization mechanisms, due to the inherently small ponderomotive shifts of short-wavelength radiation [47,49]. Here, we propose that the usage of two-color fields, composed of XUV and IR parts, make the study of dynamical interference experimentally feasible with XUV fields from HHG or FEL sources. The reason for this is that the flux and the ponderomotive shift of photoelectrons are not constrained by a single field, as previously considered in Refs. [47–49,67], but rather separately controlled by tuning the IR and XUV fields independently. In Fig. 5(a) we show that strong dynamical interference is observed when the IR intensity is increased from 1×10^{11} to 5×10^{12} W/cm^2. At the high intensity, both TDCIS-TRK (solid black) and length-gauge TDCIS (dashed orange) are in good agreement with the classical estimated energy shift: $U_p/\sqrt{2}$. The energy difference between the peak maxima of the two numerical results is 3.9% of the classical estimated energy shift.

The laser-assisted dynamical interference pattern can be studied further by choosing two different envelopes for the XUV and IR pulses, as shown in Fig. 5(b), with a peak IR intensity of 5×10^{12} W/cm^2. The dramatic change of the interference pattern is the result of the different ponderomotive potentials of the IR field and the time-dependent photoionization triggered by the XUV field. The case with a flat-top XUV and Gaussian IR field, shown as a dotted red line in Fig. 5(b), gives an interference pattern that is rather similar to the usual dynamical interference phenomenon, shown in

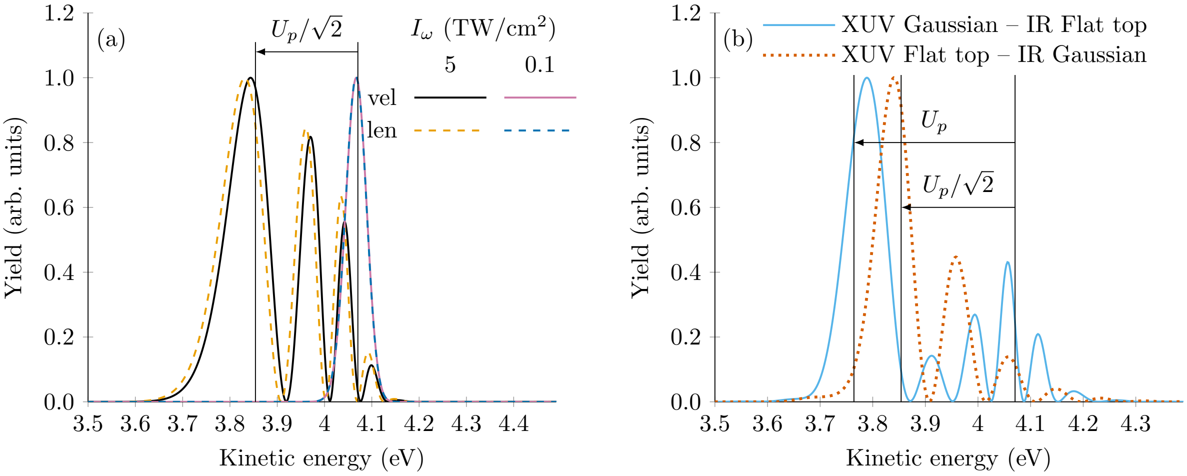

FIG. 5. Numerical demonstration of laser-assisted dynamical interference. (a) Single XUV pulse and IR pulse using truncated Gaussian envelopes. (b) Mixing flat-top and truncated Gaussian envelopes of the XUV and IR fields with $I_\omega = 5 \times 10^{12}$ W/cm^2. The expected classical energy shift is shown with an arrow and labeled U_p and $U_p/\sqrt{2}$ for a flat-top envelope and a Gaussian envelope, respectively.

Fig. 5(a), with peaks on the blue side that decrease monotonically in magnitude and increase in oscillation rate with kinetic energy. The case with a Gaussian XUV and flat-top IR field, shown in blue in Fig. 5(b), displays a more significant shift of the main peak, as expected for flat-top IR fields using classical arguments. The interference fringes on the higher kinetic energy side, however, exhibit a qualitatively different behavior with nonmonotonic peaks. We interpret this effect as Ramsey-like fringes from unshifted photoemission by the XUV pulse before and after the flat-top IR field is present. The observed Ramsey fringes are $\hbar\Delta\omega_{\mathrm{R}} \approx 60$ meV; given $2\pi = \Delta\omega_{\mathrm{R}} T$, this implies a time separation of $T \approx 64$ fs. We note that this separation is larger than the pulse duration of the flat-top IR field (35 fs), by almost a factor of 2, which we interpret as a result of the temporal spread of the XUV Gaussian flank distributions (from ±17.5 fs to $\pm\infty$) with mean values at ±29 fs.

V. CONCLUSIONS

In this article, we discussed the velocity-gauge problem of TDCIS theory. It was shown that the velocity gauge is size inconsistent, with respect to the number of active core orbitals, due to the lack of virtual transitions to doubles. An effective potential was introduced to account for nonresonant core polarization by usage of TRK theory. The simulated photoelectrons from TDCIS-TRK theory were found to agree well with those from length-gauge TDCIS, with a low number of angular momenta being required for numerical convergence of laser-assisted photoionization. Formally, there is no justification to claim that gauge invariance is achieved, but the TDCIS-TRK theory seems to perform at a level comparable to the length-gauge TDCIS, with reasonable energy shifts obtained for photoelectrons. Contrary to previous attempts to achieve full gauge invariance in TDCIS between the length gauge and the velocity gauge of TDCIS [45], the present correction can be implemented with negligible numerical cost in propagation with a spectral representation of the wave function, which may prove important for efficient implementations of TDCIS for more complex targets, such as molecules or heavy atoms.

Interestingly, the TDCIS-TRK simulations were essentially converged with the active core space limited to $\{2p\}$ in neon atoms at the considered field parameters. While this may seem reasonable at first glance, because laser-assisted photoionization processes from $2p$ are known to be weakly correlated with $2s$ in the length gauge [14], the present theory was derived from the velocity gauge, where the convergence of many-body effects in laser fields are much more subtle [15]. As an example, we showed that convergence of the effective number of active electrons, $\tilde{N} \rightarrow N$, was only reached for the *full* active core within RPAE (Table I).

In summary, the TDCIS-TRK theory allows for a reduced number of angular momenta and an efficient frozen space in time-dependent simulations of laser-assisted photoionization. The theory was used to predict an alternative type of dynamical interference phenomenon for atoms, under experimentally viable conditions, by separately controlling the flux and the ponderomotive shift by two-color fields. In future works, the TDCIS-TRK theory may prove useful for studies of other observables, such as attosecond time delays in photoionization with strongly driven resonant transitions, HHG with multiple active channels, interferometric above-threshold ionization processes, and photoionization dynamics by intense attosecond pulse trains generated by seeded FELs.

ACKNOWLEDGMENTS

J.M.D. acknowledges support from the Swedish Research Council (Grant No. 2018-03845 and No. 2020-03315), the Olle Engkvist Foundation (Grant No. 194-0734), and the Knut and Alice Wallenberg Foundation (Grants No. 2017.0104 and No. 2019.0154. We thank Andrea Idini for fruitful discussions about many-body treatment, and we thank Per Eng-Johnsson and Anne L'Huillier for fruitful discussions about laser-assisted dynamical interference.

APPENDIX: NUMERICAL SPECIFICATIONS

Our calculations of laser-assisted photoionization are performed using the vector potential

$$A(t) = [A_{0,\Omega} \sin(\Omega t) + A_{0,\omega} \sin(\omega t)] f(t), \tag{A1}$$

with $\hbar\omega = 1.530\,67\,\mathrm{eV}$ and $\hbar\Omega = 27.211\,386\,\mathrm{eV}$. To maintain the notion of a constant ponderomotive energy, while alleviating the spectral profile of the electric field, we use a flat-top pulse with smooth but sufficiently rapid truncation, given by

$$f(t) = \begin{cases} 1, & |t| \leqslant \frac{\tau}{2}, \\ \exp\left[-\tan\left(\pi \frac{|t|-\frac{\tau}{2}}{t_{\max}-\tau}\right)^2\right], & \frac{\tau}{2} < |t| \leqslant \frac{t_{\max}}{2}, \\ 0, & \text{otherwise.} \end{cases} \tag{A2}$$

This envelope is equal to unity for a width of τ and is smoothly suppressed between $|\tau|/2$ and $|t_{\max}|/2$. The width of the pulses is set to $\tau = 33.88$ fs and the smooth suppression starts at $t_{\max} = 35\,\mathrm{fs}$.

In our last example, we, however, make use of more realistic truncated Gaussian pulses, adapted from Ref. [68]. In this case, the vector potential envelope is given by

$$f(t) = \begin{cases} \exp[-\alpha t^2], & |t| \leqslant t_{\mathrm{off}}, \\ \exp\left\{-\alpha\left[t_{\mathrm{off}} + \frac{2}{\pi}(t_{\max} - t_{\mathrm{off}}) \tan\left(\frac{\pi}{2} \frac{|t|-t_{\mathrm{f}}}{t_{\max}-t_{\mathrm{f}}}\right)\right]^2\right\}, & \tau_{\mathrm{off}} < |t| \leqslant t_{\max}, \\ 0, & \text{otherwise,} \end{cases} \tag{A3}$$

where $\alpha = 2\ln 2/\tau^2$ is chosen such that the pulse length, expressed as full width at half maximum, is specified for the intensity profile of the pulse. This is valid in the long-wavelength limit. The vector potential follows a Gaussian profile within the width, specified in terms of standard deviations of the intensity profile, $\sigma = T/(2\sqrt{2\ln 2})$, of $|t| \leqslant t_{\text{off}} = 4\sigma$, and is truncated at $t_{\max} = 6\sigma$.

To resolve the photoelectron spectra we use the time-dependent surface flux [44,69] (t-SURFF) and the infinite-time surface flux [55,70] (iSURF) methods. A limiting assumption of t-SURFF is that the total wave function be separable into a bound ionic part and a free electronic part. This assumption breaks due to the long-range Coulomb potential, which scales with the inverse of the radial distance in space. However, the photoelectrons are recorded at $R_0 = 100$ bohr, where the effect of the Coulomb potential is sufficiently small to not affect our results.

[1] F. Krausz and M. Ivanov, Rev. Mod. Phys. **81**, 163 (2009).

[2] F. Calegari, A. Trabattoni, A. Palacios, D. Ayuso, M. C. Castrovilli, J. B. Greenwood, P. Decleva, F. Martín, and M. Nisoli, J. Phys. B: At., Mol. Opt. Phys. **49**, 142001 (2016).

[3] S. Ghimire and D. A. Reis, Nat. Phys. **15**, 10 (2019).

[4] M. Isinger, R. J. Squibb, D. Busto, S. Zhong, A. Harth, D. Kroon, S. Nandi, C. L. Arnold, M. Miranda, J. M. Dahlström, E. Lindroth, R. Feifel, M. Gisselbrecht, and A. L'Huillier, Science **358**, 893 (2017).

[5] P. M. Paul, E. S. Toma, P. Breger, G. Mullot, F. Augé, P. Balcou, H. G. Muller, and P. Agostini, Science **292**, 1689 (2001).

[6] M. Schultze, M. Fieß, N. Karpowicz, J. Gagnon, M. Korbman, M. Hofstetter, S. Neppl, A. L. Cavalieri, Y. Komninos, T. Mercouris, C. A. Nicolaides, R. Pazourek, S. Nagele, J. Feist, J. Burgdörfer, A. M. Azzeer, R. Ernstorfer, R. Kienberger, U. Kleineberg, E. Goulielmakis *et al.*, Science **328**, 1658 (2010).

[7] G. Laurent, W. Cao, H. Li, Z. Wang, I. Ben-Itzhak, and C. L. Cocke, Phys. Rev. Lett. **109**, 083001 (2012).

[8] P. K. Maroju, C. Grazioli, M. D. Fraia, M. Moioli, D. Ertel, H. Ahmadi, O. Plekan, P. Finetti, E. Allaria, L. Giannessi, G. D. Ninno, C. Spezzani, G. Penco, S. Spampinati, A. Demidovich, M. B. Danailov, R. Borghes, G. Kourousias, C. E. S. D. Reis, F. Billé *et al.*, Nature (London) **578**, 386 (2020).

[9] S. Haessler, B. Fabre, J. Higuet, J. Caillat, T. Ruchon, P. Breger, B. Carré, E. Constant, A. Maquet, E. Mével, P. Salières, R. Taïeb, and Y. Mairesse, Phys. Rev. A **80**, 011404(R) (2009).

[10] A. L. Wang, V. V. Serov, A. Kamalov, P. H. Bucksbaum, A. Kheifets, and J. P. Cryan, Phys. Rev. A **104**, 063119 (2021).

[11] A. L. Cavalieri, N. Müller, T. Uphues, V. S. Yakovlev, A. Baltuška, B. Horvath, B. Schmidt, L. Blümel, R. Holzwarth, S. Hendel, M. Drescher, U. Kleineberg, P. M. Echenique, R. Kienberger, F. Krausz, and U. Heinzmann, Nature (London) **449**, 1029 (2007).

[12] S. Neppl, R. Ernstorfer, A. L. Cavalieri, C. Lemell, G. Wachter, E. Magerl, E. M. Bothschafter, M. Jobst, M. Hofstetter, U. Kleineberg, J. V. Barth, D. Menzel, J. Burgdörfer, P. Feulner, F. Krausz, and R. Kienberger, Nature (London) **517**, 342 (2015).

[13] M. Bertolino and J. M. Dahlström, Phys. Rev. Res. **3**, 013270 (2021).

[14] J. M. Dahlström, T. Carette, and E. Lindroth, Phys. Rev. A **86**, 061402(R) (2012).

[15] J. Vinbladh, J. M. Dahlström, and E. Lindroth, Phys. Rev. A **100**, 043424 (2019).

[16] D. Baykusheva and H. J. Wörner, J. Chem. Phys. **146**, 124306 (2017).

[17] A. Kamalov, A. L. Wang, P. H. Bucksbaum, D. J. Haxton, and J. P. Cryan, Phys. Rev. A **102**, 023118 (2020).

[18] J. Benda, Z. Mašín, and J. D. Gorfinkiel, Phys. Rev. A **105**, 053101 (2022).

[19] Á. Jiménez-Galán, L. Argenti, and F. Martín, Phys. Rev. Lett. **113**, 263001 (2014).

[20] Á. Jiménez-Galán, F. Martín, and L. Argenti, Phys. Rev. A **93**, 023429 (2016).

[21] M. Kotur, D. Guénot, Á. Jiménez-Galán, D. Kroon, E. W. Larsen, M. Louisy, S. Bengtsson, M. Miranda, J. Mauritsson, C. L. Arnold, S. E. Canton, M. Gisselbrecht, T. Carette, J. M. Dahlström, E. Lindroth, A. Maquet, L. Argenti, F. Martín, and A. L'Huillier, Nat. Commun. **7**, 10566 (2016).

[22] V. Gruson, L. Barreau, Á. Jiménez-Galan, F. Risoud, J. Caillat, A. Maquet, B. Carré, F. Lepetit, J.-F. Hergott, T. Ruchon, L. Argenti, R. Taïeb, F. Martín, and P. Salières, Science **354**, 734 (2016).

[23] L. Argenti, Á. Jiménez-Galán, J. Caillat, R. Taïeb, A. Maquet, and F. Martín, Phys. Rev. A **95**, 043426 (2017).

[24] L. Barreau, C. L. M. Petersson, M. Klinker, A. Camper, C. Marante, T. Gorman, D. Kiesewetter, L. Argenti, P. Agostini, J. González-Vázquez, P. Salières, L. F. DiMauro, and F. Martín, Phys. Rev. Lett. **122**, 253203 (2019).

[25] J. Parker, K. T. Taylor, C. W. Clark, and S. Blodgett-Ford, J. Phys. B: At., Mol. Opt. Phys. **29**, L33 (1996).

[26] M. Ossiander, F. Siegrist, V. Shirvanyan, R. Pazourek, A. Sommer, T. Latka, A. Guggenmos, S. Nagele, J. Feist, J. Burgdörfer, R. Kienberger, and M. Schultze, Nat. Phys. **13**, 280 (2017).

[27] N. Rohringer, A. Gordon, and R. Santra, Phys. Rev. A **74**, 043420 (2006).

[28] L. Greenman, P. J. Ho, S. Pabst, E. Kamarchik, D. A. Mazziotti, and R. Santra, Phys. Rev. A **82**, 023406 (2010).

[29] A. C. Brown, G. S. J. Armstrong, J. Benda, D. D. A. Clarke, J. Wragg, K. R. Hamilton, Z. Mašín, J. D. Gorfinkiel, and H. W. van der Hart, Comput. Phys. Commun. **250**, 107062 (2020).

[30] J. Benda, J. D. Gorfinkiel, Z. Mašín, G. S. J. Armstrong, A. C. Brown, D. D. A. Clarke, H. W. van der Hart, and J. Wragg, Phys. Rev. A **102**, 052826 (2020).

[31] C. Marante, M. Klinker, T. Kjellsson, E. Lindroth, J. González-Vázquez, L. Argenti, and F. Martín, Phys. Rev. A **96**, 022507 (2017).

[32] T. Sato and K. L. Ishikawa, Phys. Rev. A **91**, 023417 (2015).

[33] H. Miyagi and L. B. Madsen, Phys. Rev. A **87**, 062511 (2013).

[34] H. Miyagi and L. B. Madsen, Phys. Rev. A **89**, 063416 (2014).

[35] A. D. Bandrauk, F. Fillion-Gourdeau, and E. Lorin, J. Phys. B: At., Mol. Opt. Phys. **46**, 153001 (2013).

[36] K. L. Ishikawa and T. Sato, IEEE J. Sel. Top. Quantum Electron. **21**, 1 (2015).

[37] M. Wolfsberg, J. Chem. Phys. **23**, 793 (1955).

[38] D. H. Kobe, Phys. Rev. A **19**, 205 (1979).

[39] D. H. Kobe and A. L. Smirl, Am. J. Phys. **46**, 624 (1978).

[40] H. R. Reiss, Prog. Quantum Electron. **16**, 1 (1992).

[41] E. Cormier and P. Lambropoulos, J. Phys. B: At., Mol. Opt. Phys. **29**, 1667 (1996).

[42] H. G. Muller, Laser Phys. **9**, 138 (1999).

[43] K. J. Schafer, Numerical methods in strong field physics, in *Strong Field Laser Physics*, edited by T. Brabec, Springer Series in Optical Sciences Vol. 134 (Springer, New York, 2009), pp. 111–145.

[44] M. Bertolino, D. Busto, F. Zapata, and J. M. Dahlström, J. Phys. B: At., Mol. Opt. Phys. **53**, 144002 (2020).

[45] T. Sato, T. Teramura, and K. L. Ishikawa, Appl. Sci. **8**, 433 (2018).

[46] W. Kuhn, Z. Phys. **33**, 408 (1925).

[47] K. Toyota, O. I. Tolstikhin, T. Morishita, and S. Watanabe, Phys. Rev. A **76**, 043418 (2007).

[48] M. Baghery, U. Saalmann, and J. M. Rost, Phys. Rev. Lett. **118**, 143202 (2017).

[49] W.-C. Jiang and J. Burgdörfer, Opt. Express **26**, 19921 (2018).

[50] J. J. Sakurai and J. Napolitano, *Modern Quantum Mechanics*, 2nd ed. (Cambridge University, Cambridge, England, 2017).

[51] H. Bethe and E. Salpeter, *Quantum Mechanics of One- and Two-Electron Atoms* (Plenum, New York, 1977).

[52] H. Margenau, Phys. Rev. **56**, 1000 (1939).

[53] P. H. Bucksbaum, R. R. Freeman, M. Bashkansky, and T. J. McIlrath, J. Opt. Soc. Am. B **4**, 760 (1987).

[54] V. S. Yakovlev and M. S. Wismer, Comput. Phys. Commun. **217**, 82 (2017).

[55] S. Carlström, M. Spanner, and S. Patchkovskii, Phys. Rev. A **106**, 043104 (2022).

[56] S. Carlström, M. Bertolino, J. M. Dahlström, and S. Patchkovskii, Phys. Rev. A **106**, 042806 (2022).

[57] F. Zapata, J. Vinbladh, A. Ljungdahl, E. Lindroth, and J. M. Dahlström, Phys. Rev. A **105**, 012802 (2022).

[58] S. Pabst, L. Greenman, D. A. Mazziotti, and R. Santra, Phys. Rev. A **85**, 023411 (2012).

[59] J. Olsen, B. O. Roos, P. Jo/rgensen, and H. J. A. Jensen, J. Chem. Phys. **89**, 2185 (1988).

[60] D. Hochstuhl and M. Bonitz, Phys. Rev. A **86**, 053424 (2012).

[61] I. Lindgren and J. Morrison, *Atomic Many-Body Theory*, 2nd ed., Springer Series on Atomic, Optical, and Plasma Physics (Springer-Verlag, Berlin, 1986).

[62] M. Y. Amusia, *Atomic Photoeffect*, Springer Series on Physics of Atoms and Molecules (Springer, New York, 1990).

[63] H. Friedrich, *Theoretical Atomic Physics*, 1st ed. (Springer, Berlin, 1991).

[64] B. L. Beers and L. Armstrong, Phys. Rev. A **12**, 2447 (1975).

[65] C. R. Holt, M. G. Raymer, and W. P. Reinhardt, Phys. Rev. A **27**, 2971 (1983).

[66] A. Karamatskou, S. Pabst, Y.-J. Chen, and R. Santra, Phys. Rev. A **89**, 033415 (2014).

[67] R. Della Picca, A. A. Gramajo, C. R. Garibotti, S. D. López, and D. G. Arbó, Phys. Rev. A **93**, 023419 (2016).

[68] S. Patchkovskii and H. G. Muller, Comput. Phys. Commun. **199**, 153 (2016).

[69] L. Tao and A. Scrinzi, New J. Phys. **14**, 013021 (2012).

[70] F. Morales, T. Bredtmann, and S. Patchkovskii, J. Phys. B: At., Mol. Opt. Phys. **49**, 245001 (2016).